ACS OMEGA

http://pubs.acs.org/journal/acsodf

Article

Fabrication of Hydrogels via Host–Guest Polymers as Highly Efficient Organic Dye Adsorbents for Wastewater Treatment

Nan Hou, Ran Wang, Fan Wang, Jiahui Bai, Jingxin Zhou,* Lexin Zhang, Jie Hu, Shufeng Liu, and Tifeng Jiao*

Cite This: *ACS Omega* 2020, 5, 5470–5479

Read Online

ACCESS | Metrics & More | Article Recommendations

ABSTRACT: New self-assembled hydrogel materials of poly(vinyl alcohol)/cyclodextrin-modified poly(acrylic acid)/azobenzene-modified poly(acrylic acid) (PVA/PAA-CD/PAA-Azo) were successfully prepared via host–guest interactions and hydrogen bonds. The as-prepared hydrogel materials were characterized by various techniques, including Fourier transform infrared spectroscopy, X-ray diffraction analysis, scanning electron microscopy, ultraviolet spectroscopy, and specific surface area tests. The prepared hydrogels with different concentrations of PVA exhibited different network structures. In addition, ultraviolet (UV) light irradiation and temperature change induce a gel–sol phase transition in the hydrogel materials. The obtained hydrogel materials could be used as good adsorbents for two model organic dye molecules, which was mainly due to electrostatic interactions between methylene blue/rhodamine B (MB/RhB) and the gels in the adsorption process. In particular, the adsorption processes of the as-prepared hydrogel materials conformed to the pseudo-first-order model with a high correlation coefficient, which indicates that gel has a potential application in the field of wastewater purification.

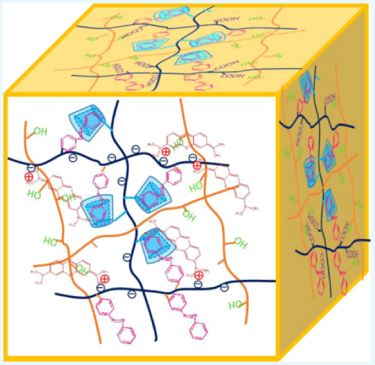

1. INTRODUCTION

Hydrogels have been widely researched in material fields, such as drug delivery systems,[1,2] biosensors,[3] tissue engineering,[4] and wastewater treatment.[5,6] The mechanical properties and stimulus response of hydrogels play a key role in their application.[7,8] By designing unique structures or introducing reversible bonds into the hydrogel network, the practical application of hydrogels can be greatly improved.[9,10] It is difficult for conventional polymer network hydrogels to achieve stimulus response because they do not re-form covalent bonds. One of the most facile methods for preparing supramolecular hydrogels is the formation of a noncovalent system using host–guest interactions,[11] hydrogen bonding,[12] $\pi-\pi$ stacking interactions,[13] or ion interactions.[14] In all noncovalent interactions, the host–guest interaction has been widely used to prepare supramolecular materials.[15−18]

In host–guest systems, cyclodextrins (CDs) are ideal host molecules because they have a conical hollow special structure with a hydrophilic exterior edge and a hydrophobic interior cavity.[19] Cyclodextrin is composed of six, seven, or eight repeated monomers of glucopyranose units linked by α-1,4-glycosidic linkages, called α-, β-, and γ-CD, respectively.[20] β-CD, as one of the most commonly used derivatives, has attracted much attention due to its easy acquirement, moderate internal diameter, and good modifiability. In addition, a well-controlled clathrate can be easily obtained by the modification of azobenzene to an ideal guest of β-CD. Azobenzene has cis and trans spatial structures with significant differences in molecular size and dipole moment. Reversible cis–trans isomerization of azobenzene is induced based on light irradiation at different wavelengths, leading to the reversible assembly of clathrates, which may affect the macroscopic behavior of the material.[21,22]

Recently, supramolecular gels have received much attention as highly efficient and economical adsorbents for adsorbing harmful contaminants.[23,24] For example, Thakur and coworkers reported a sodium alginate-based organic/inorganic super-absorbent composite hydrogel for the adsorption of methylene blue (MB).[25] The porous three-dimensional (3D) network structure inside the hydrogel provides a large surface area and a large number of channels, thereby providing abundant channels and numerous adsorption sites for the dispersion of dye solution.[26−29] For example, Pandey et al. reported natural locust bean gum-based hydrogels as good adsorbents for the removal of dyes from an aqueous solution.[27] Marandi and coworkers reported a poly(AA-*co*-VPA) hydrogel as a potent adsorbent for the adsorption of dye.[30] Hu et al. reported a PAA-based superadsorbent hydrogel for the removal of MB.[31] In general,

Received: January 7, 2020
Accepted: February 24, 2020
Published: March 5, 2020

https://dx.doi.org/10.1021/acsomega.0c00076
ACS Omega 2020, 5, 5470–5479

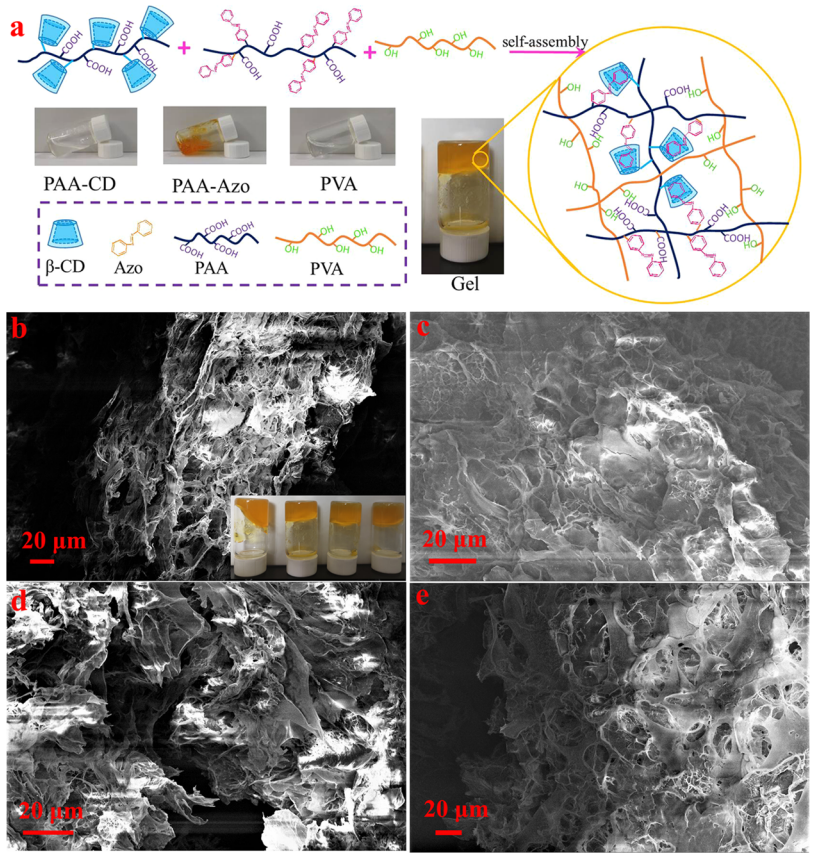

Figure 1. (a) Schematic illustration of hydrogel formation. Scanning electron microscope (SEM) image of as-obtained PVA/PAA-CD/PAA-Azo hydrogels: (b) Gel-A, (c) Gel-B, (d) Gel-C, and (e) Gel-D. Photograph courtesy of "Nan Hou." Copyright 2020.

Table 1. Concentration Ratios of PVA, PAA-CD, and PAA-Azo in Hydrogels

	PAA-CD concn [mg/mL]/volume [mL]	PAA-Azo concn [mg/mL]/volume [mL]	PVA concn [mg/mL]/volume [mL]
Gel-A	20/0.5	20/0.5	12.5/1
Gel-B	20/0.5	20/0.5	25/1
Gel-C	20/0.5	20/0.5	37.5/1
Gel-D	20/0.5	20/0.5	50/1

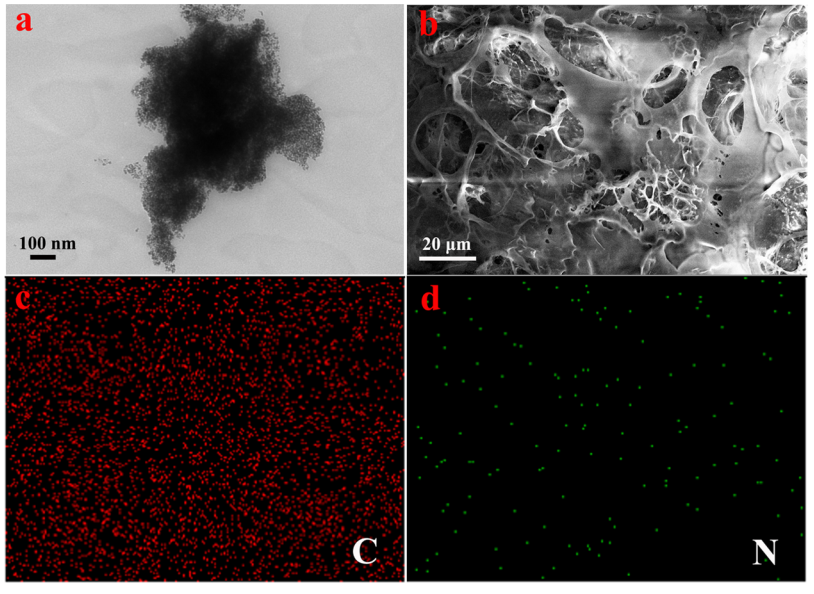

Figure 2. (a) Transmission electron microscopy (TEM) images of Gel-D; (b) EDS elemental maps of Gel-D (b–d).

https://dx.doi.org/10.1021/acsomega.0c00076
ACS Omega 2020, 5, 5470−5479

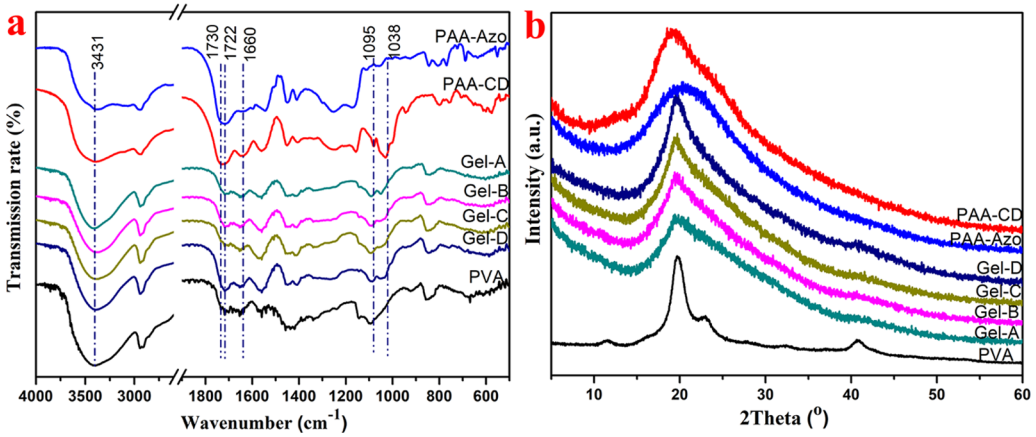

Figure 3. (a) FT-IR spectra of PVA, PAA-CD, PAA-Azo, and hydrogels; (b) X-ray diffraction (XRD) patterns PVA, PAA-CD, PAA-Azo, and hydrogels.

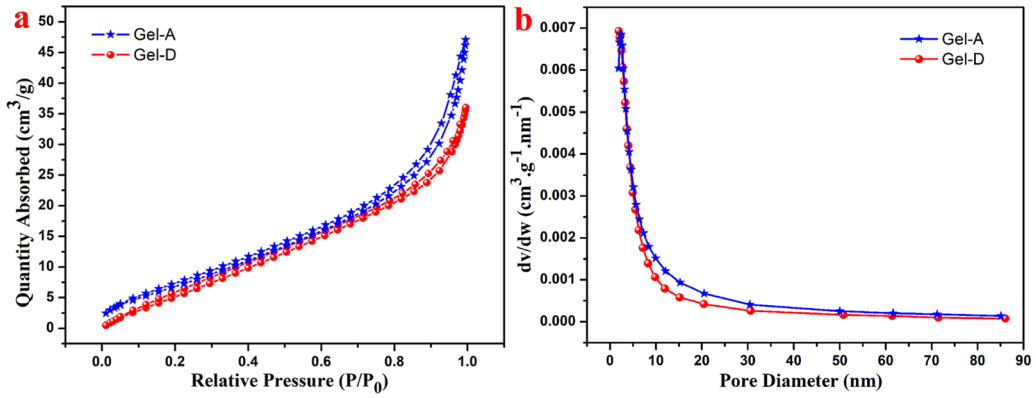

Figure 4. (a) N_2 adsorption−desorption isotherms; (b) pore size distribution of the obtained hydrogels.

most of the previously reported dye adsorbent materials exhibit some disadvantages, such as complicated preparation, toxic raw materials, poor stability, and weak adsorption capacity.[23,32] Therefore, in practical applications, it is still a challenge to manufacture an adsorbent highly efficient and capable to rapidly remove dyes, with good mechanical stability and ecofriendly preparation.

In this study, we designed and synthesized a novel hydrogel material using poly(vinyl alcohol), azobenzene-modified poly(acrylic acid), and cyclodextrin-modified poly(acrylic acid) (PVA/PAA-CD/PAA-Azo). The formations of hydrogels were mainly driven by host−guest interactions and hydrogen bonding, as shown in Figure 1a. Moreover, ultraviolet (UV) light irradiation and temperature change induce a gel−sol phase transition in the hydrogel material. In addition, the obtained hydrogels show excellent adsorption performance and potential application in removing organic dyes and wastewater purification.

2. RESULTS AND DISCUSSION

2.1. Preparation and Characterization of Hydrogel. Herein, the inset of Figure 1b shows a photo of the hydrogels. It can be seen that the four sets of hydrogels show excellent gel stability, and with the increasing concentration of PVA, the hydrogel becomes more and more stable (Table 1). Figure 1b−e shows the microstructures of the freeze-dried samples. According to SEM, it can be observed that all xerogels exhibit a three-dimensional porous network structure. The pore sizes of the network are in the range of nanometers to several micrometers, and the interconnected porous represent areas filled with water. On comparing the xerogels, it could be seen that the size of pores and the cross-link density vary with the PVA concentration. Due to the increase in the concentration of PVA in hydrogels, the cross-link density in the gel increases. To further explore the microstructures of the gel, Gel-D was analyzed using transmission electron microscopy (TEM) and SEM combined with energy-dispersive X-ray spectroscopy (EDS) to determine the elements present in the hydrogel, as shown in Figure 2. The obtained TEM images of the hydrogel further indicated that porous 3D network nanostructures were formed by the self-assembly process. It could be seen that the formed gel was a slit pore material composed by the accumulation of platelike particles with pores in several nanometer sizes. The corresponding elemental mapping analyses of Gel-D are shown in Figure 2b−d. EDS elemental maps reveal that the compositional distributions of the two elements (C, N) in Gel-D are uniform. It can be seen that the N element mapping is weak due to the small amount of 4-aminoazobenzene- and NH_2-β-CD-modified PAA (0.05 equiv of the acrylic acid unit). The element mapping images demonstrate that the pore walls consist of thin layers of PAA-CD, PAA-Azo, and PVA, due to the host−guest interaction between CD and Azo, which results in hydrogel formation.

To characterize structural changes in the gels, Fourier transform infrared (FT-IR) spectra of PAA-CD, PAA-Azo, PVA, and four sets of hydrogels (Gel-A, Gel-B, Gel-C, and Gel-

https://dx.doi.org/10.1021/acsomega.0c00076
ACS Omega 2020, 5, 5470−5479

D) were further collected, as shown in Figure 3a. For PVA, the absorption band at 3431 cm^{-1} is ascribed to the hydroxyl group (O−H) stretching vibration. For the PAA-CD, the characteristic peaks at 1730 cm^{-1} were attributed to the stretching vibration of the carbonyl group. Moreover, for the hydrogel, the absorption band at 1730 cm^{-1} assigned to the stretching vibration of the carbonyl group in PAA shifts to around 1722 cm^{-1} in the gel, suggesting the formation of relatively weaker C═O---H−O hydrogen bonds between PVA and PAA chains.[12] The peak at 1038 cm^{-1} was ascribed to the vibration of the C−O−C bond. Furthermore, the peak at 1095 cm^{-1} was attributed to C−OH bonds. The absorption peak at 2920 cm^{-1} represents the antisymmetric absorption of the $-CH_2$ group.

Next, the obtained PAA-CD, PAA-Azo, PVA, and four sets of hydrogels (Gel-A, Gel-B, Gel-C, and Gel-D) were characterized by the XRD pattern in the 2θ range of 0−60, and the results are shown in Figure 3b. The XRD pattern of PAA-CD and PAA-Azo has a broad peak with a position of 19 and 21°, respectively, which is mainly attributed to the alkyl main chain in the PAA molecule; PAA-CD and PAA-Azo were in an amorphous state. In the XRD pattern of PVA, a sharp crystalline peak at a 2θ value of 19.31 and a shoulder peak at a 2θ value of 22.61 correspond to the (101) and (200) planes of PVA crystallites.[33] All hydrogels show sharp diffraction peaks at a 2θ value of 19.31, and the crystallinity of the hydrogel gradually increases with the increase of the PVA concentration, suggesting that the introduction of PVA chains into gels can increase the crystallinity of the gels.

Furthermore, the porous microstructure of the obtained xerogels was further investigated by utilizing the nitrogen adsorption−desorption isotherms, as shown in Figure 4a. The experimental data of the samples are shown in Table 2. The

Table 2. Physical Data of the Obtained Gel-A and Gel-D

sample	specific surface area (m^2/g)	average pore diameter (nm)	pore volume (cm^3/g)
Gel-A	27.77	7.87	0.068307
Gel-D	29.96	6.49	0.050609

adsorption isotherms of xerogels are S-type, which means that the adsorption process occurs on macroporous solids. Within the pressure range tested, the hysteresis loops of xerogels are type IV isotherm curves observed at a higher relative pressure (P/P_0 = 0.80−0.95), indicating the presence of a macroporous structure. These two hysteresis loops can be divided into H3 or H4 hysteresis effect, indicating that the formed gel adsorbent is a slit pore material formed by the accumulation of platelike particles. In addition, the Barrett−Joyner−Halenda (BJH) method was also used to calculate the pore size distribution of the gel and the results can be seen in Figure 4b. Gel-D has a higher BET specific surface area of 29.96 m^2/g, while Gel-A has an area of 27.77 m^2/g. The order of the pore volume and average pore diameter was Gel-A > Gel-D, which indicated that as the amount of PVA increased, the cross-linking density of the hydrogel became larger.

It is well known that azobenzene compounds exhibit typical trans−cis isomerization under ultraviolet irradiation and show unfavorable cis−trans isomerization under visible light.[32,34] β-CD and its derivatives can only form inclusion complexes with trans Azo molecules, which are mainly governed by hydrophobic interactions. The photoisomerization performances of the azobenzene group were studied using Gel-D, as shown in Figure 5. Figure 5c shows the ultraviolet−visible (UV−vis) absorption spectra of Gel-D with the irradiation time of 0 s, 10 s, 20 s, 30 s, 1 min, and 5 min. The major absorption peak at 348 nm was assigned to the $\pi-\pi$ electronic transition of the azobenzene trans-isomer, whereas that at 438 nm was assigned to the electronic transition of the cis-isomer. With the increment of ultraviolet irradiation time, the $\pi-\pi$ transition peak intensity gradually decreases and the n−π transition peak intensity gradually increases, which confirms the trans-to-cis isomerization of the azobenzene group. Therefore, supramolecular hydrogels undergo gel−sol transitions under UV light (λ = 365 nm). When excluded from the CD cavity, the cross-linked inclusion complex dissociated within a certain time. After leaving the sol state in visible light (λ = 450 nm for about 24 h), the conformation of the azobenzene unit was slowly isomerized from cis to trans in the complex, which induced the reconstruction of the cross-linked network and the coagulation gel recovery.[21] Finally, we investigated the effect of temperature on the phase transition of supramolecular hydrogels, as shown in Figure 6. When the gel is heated to 90 °C, hydrogen bonds are broken and the bonding strength between the host and the guest is impaired, resulting in the formation of a liquid solution. Once gradually cools to room temperature, the supramolecular cross-linked network slowly regenerates and restores the solution to a gel state.

2.2. Adsorption Performances in Dye Removal. The porous microstructure of the currently prepared hydrogel provides it with excellent mechanical strength and large specific

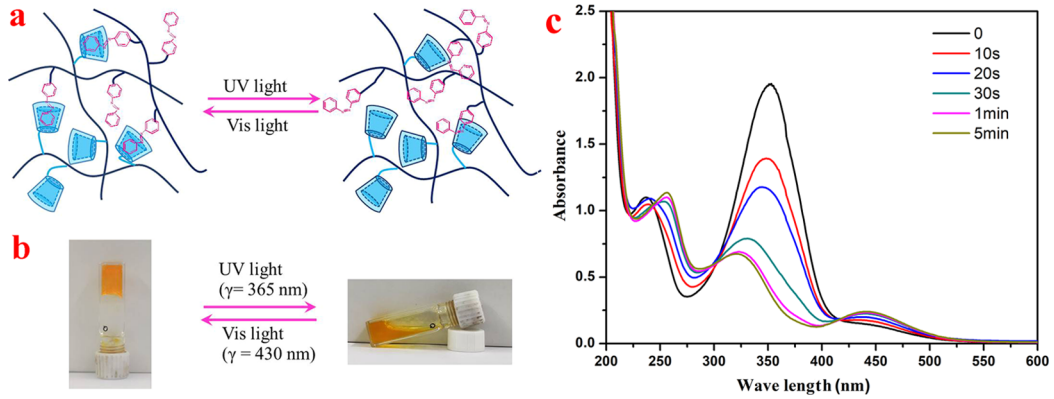

Figure 5. (a) Schematic illustration of sol−gel transition; (b) sol−gel transition experiment using light irradiation; and (c) UV−vis spectra of Gel-D by exposure to UV light. Photograph courtesy of Nan Hou. Copyright 2020.

https://dx.doi.org/10.1021/acsomega.0c00076
ACS Omega 2020, 5, 5470−5479

Figure 6. Reversible sol−gel transition of Gel-D induced by temperature stimuli. Photograph courtesy of Nan Hou. Copyright 2020.

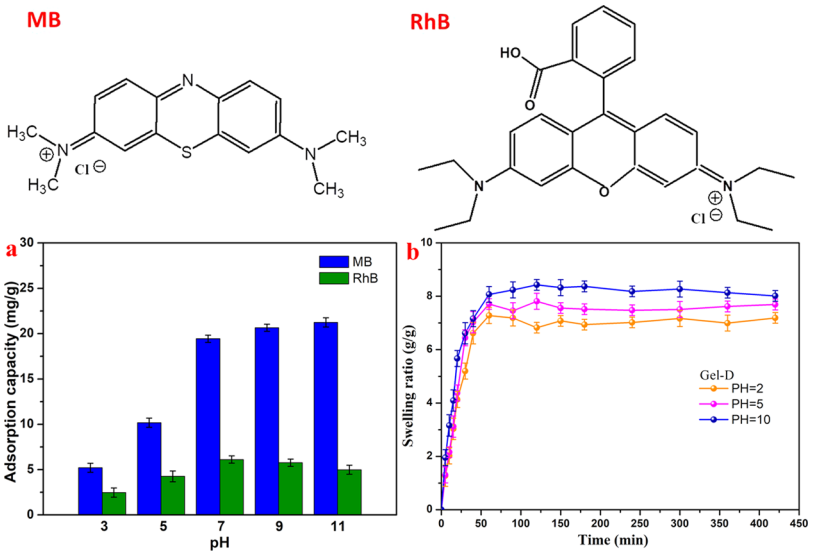

Figure 7. Molecular structures of two dyes. (a) Effect of pH on the adsorption capacity of Gel-D. (b) Swelling kinetics of Gel-D.

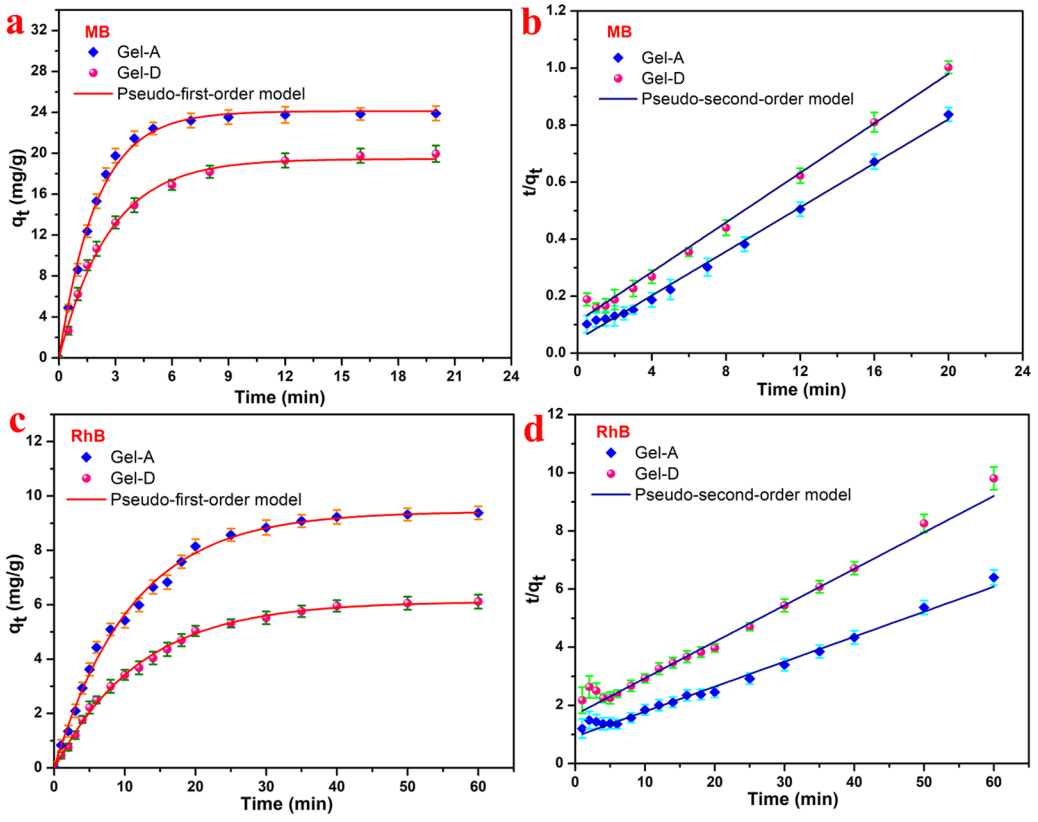

Figure 8. Adsorption kinetics (a) q_t versus t plots and (b) t/q_t versus t plots for MB and (c) q_t versus t plots and (d) t/q_t versus t plots for RhB.

surface area, which are advantageous for adsorption experiments. The pH of the dye solution plays an important role in the adsorption process. By controlling the pH value of the dye solution, we can understand the effect of electrostatic

https://dx.doi.org/10.1021/acsomega.0c00076
ACS Omega 2020, 5, 5470−5479

Table 3. Kinetic Parameters of Obtained Gel-A and Gel-D for MB and RhB Removal at 298 K

		pseudo-first-order model			pseudo-second-order model		
		q_e (mg/g)	R^2	K_1 (min^{-1})	q_e (mg/g)	R^2	K_2 [g/(mg min)]
MB	Gel-A	24.11	0.999	0.5007	25.86	0.994	0.0315
	Gel-D	19.44	0.998	0.3761	23.02	0.992	0.0170
RhB	Gel-A	9.43	0.996	0.0914	11.64	0.987	0.00796
	Gel-D	6.12	0.998	0.0827	7.98	0.988	0.00935

interactions on the adsorption behavior of dyes. Therefore, using NaOH or HCl solution to adjust the pH value in the range of 3−11 at room temperature, the adsorption behavior of the hydrogel adsorbent for dyes was studied (Figure 7a). In acidic solutions (pH < 5), the adsorption capacity of the hydrogel for MB and rhodamine B (RhB) was weak, but when the pH value increased from 7 to 11, the adsorption capacity of the hydrogel adsorbent gradually increased for MB and slightly reduced for RhB. The pH sensitivity was mainly attributed to two factors: at acid conditions with pH values 3−5, the protonation of COO^- to COOH groups of the polymer and the surface charge of the hydrogel adsorbent were reduced, which were unfavorable for the removal of positively charged ionic dyes. Under pH values 9−11, some of the COOH groups in the hydrogel ionized to COO^- and the surface negative charge of the gel adsorbent increased, which were beneficial for the removal of MB because the electrostatic attraction to the positively charged MB was enhanced. Some COOH groups of RhB molecules ionized to COO^-, which reduced the positive charge of dyes, which is disadvantageous for the removal of RhB. In addition, the swelling behavior of Gel-D in aqueous solution at different pH values is shown in Figure 7b. The swelling rate of Gel-D changes with the pH values of the solution, and when the pH value is increased from 2 to 10, the swelling rate of Gel-D gradually increases, indicating that the cross-linked structure of the hydrogel changed at different pH values. Considering the practical application, the adsorption capacity of the hydrogel was further tested using two organic dye molecules (MB and RhB) with pH 7. As shown in Figure 8, the prepared hydrogel shows a continuous adsorption process for MB and RhB. The adsorption equilibrium times of MB and RhB were about 8 and 30 min. The typical kinetic models were further utilized to explore the adsorption kinetics.

The pseudo-first-order model is

$$\log(q_e - q_t) = \log q_e - \frac{k_1}{2.303}t \quad (1)$$

The pseudo-second-order model is

$$\frac{t}{q_t} = \frac{1}{k_2 q_e^{\,2}} + \frac{t}{q_e} \quad (2)$$

where q_e represents the adsorption capacity at equilibrium time, q_t represents the adsorption capacity at time t, and k_1 and k_2 represent kinetic rate constants. The adsorption fitting results are listed in Table 2. The fitting data show that the gel conformed to the pseudo-first-order model with a high correlation coefficient (R^2 > 0.996) in both MB and RhB adsorption processes, which was more accurately described than the pseudo-second-order model. Comparing Gel-A and Gel-D, the adsorption capacity of Gel-A was 25.86 mg/g for MB and 11.64 mg/g for RhB. On the contrary, the adsorption capacity of Gel-D only reached 23.02 mg/g for MB and 7.98 mg/g for RhB. The larger specific surface area provided adsorption sites, which facilitates the adsorption of dye molecules. However, the obtained Gel-A exhibited better dye adsorption capacity than Gel-D, which was possibly attributed to the electrostatic interaction between MB/RhB and the gel, which is considered to be the main factor in the adsorption process.[31,35] On the other hand, the regeneration of the absorbent material is also one of the important factors. For the obtained hydrogel adsorbents, the hydrogel component during regeneration showed a slight loss after washing with a strong acid solvent, and the reusability performance does seem less optimistic (Table 3).

As we all know, the adsorption mechanism between adsorbents and pollutants includes chemical bonds, electrostatic interactions, ion exchange, hydrogen bonding, hydrophobic attraction, van der Waals forces, and physical adsorption.[36−38] In our work, MB and RhB are positively charged organic molecules, and the −COOH group in PAA in the gel can anchor MB and RhB molecules via electrostatic force and hydrogen bonding. Figure 9 illustrates the adsorption mechanism of a hydrogel. The

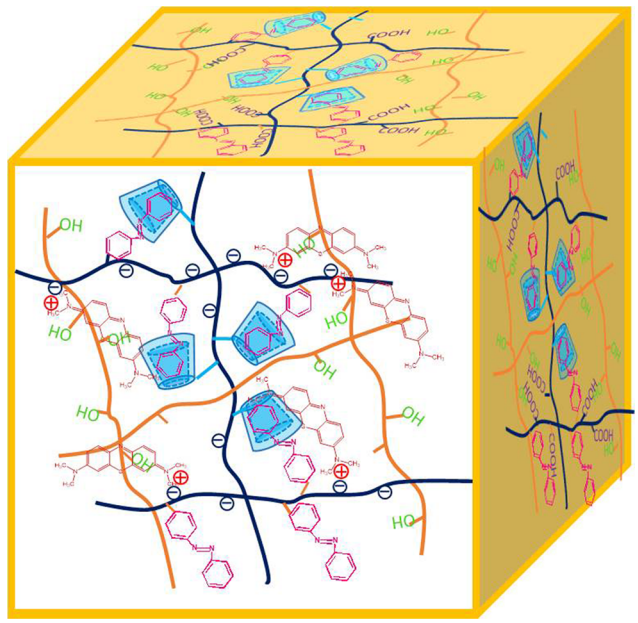

Figure 9. Schematic illustration of the Gel-D adsorption process of MB.

hydrogel has −OH, −COOH, and other hydrophilic functional groups and facilitates rapid penetration of dye solutions into the hydrogel network, which proves the removal efficiency of the prepared hydrogel. On the other hand, as the anionic structure is composed of carboxyl and amide groups in the hydrogel and as MB belongs to a positively charged organic molecule, it interacts with the −COOH group of the PAA molecular skeleton in the obtained gel through electrostatic interactions and hydrogen bonds.[39−48] In addition, from a practical point of view, the structural stability of the adsorbent is critical for water purification and environmental engineering. The microstructure

https://dx.doi.org/10.1021/acsomega.0c00076
ACS Omega 2020, 5, 5470−5479

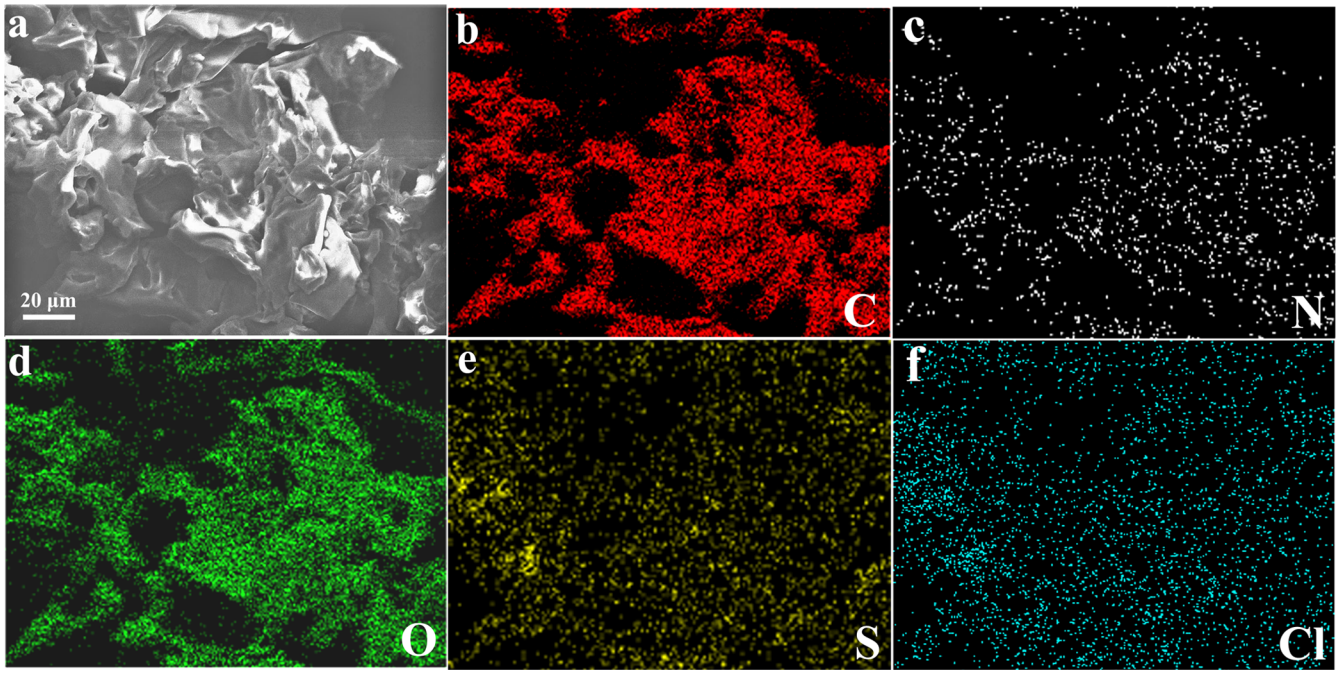

Figure 10. SEM image (a) and element mappings (b−f) of Gel-D-MB.

after MB adsorption by Gel-D was further investigated via SEM, as shown in Figure 10. It can be seen that due to the swelling of the gel, the cross-linked structure of the gel is slightly deformed after adsorption. The corresponding element distribution images of Gel-D-MB are shown in Figure 10b−f. It can be observed that S and Cl elements appear uniformly in Gel-D-MB, which means that a large number of MB molecules are adsorbed into the cross-linking network of the hydrogel. It is expected that the obtained hydrogels can be used to adsorb other cationic dye molecules, which demonstrates a new clue for the synthesis of self-assembled nanomaterials and composites.[49−58]

3. CONCLUSIONS

In summary, new supramolecular hydrogels were designed and prepared by taking advantage of the self-assembly process. The hydrogels can form good cross-linked structures without any cross-linking agent or monomer. The gel materials have porous structures, which is beneficial to increase the adsorption site of the adsorbent. The UV light irradiation experiment demonstrated the gel−sol conversion process of the supramolecular hydrogels due to the cis−trans isomerization of the azobenzene group. The prepared hydrogels showed the outstanding adsorption capacity for removing organic pollutants from wastewater. The adsorption of MB and RhB on the hydrogel adsorbent is consistent with the pseudo-first-order model. The maximum adsorption capacity can reach 25.86 mg/g for MB and 11.64 mg/g for RhB. It could be expected that other cationic dyes could also be removed by the obtained hydrogel materials. Meanwhile, this work also provides a new clue for developing self-assembled hydrogels as an efficient adsorbent for wastewater treatment.

4. EXPERIMENTAL SECTION

4.1. Materials. β-Cyclodextrin (98%, abbreviated as β-CD), poly(acrylic acid) (PAA, MW = 450 000), and 4-aminoazobenzene (abbreviated as N-Azo) were purchased from Sinopharm Chemical Reagent Co. Ltd. and TCL Shanghai Chemical Reagent Co. Ltd. (analytical reagent grade, Shanghai, China). 1-Ethyl-3-(3-dimethylaminopropyl)carbodiimide hydrochloride (EDC-HCl) and *N*-hydroxysuccinimide (NHS) were purchased from Sigma-Aldrich. Methylene blue (MB) and rhodamine B (RhB) were purchased from Sinopharm Chemical Reagent Co. Ltd. (analytical reagent grade, Shanghai, China). Poly(vinyl alcohol) (PVA) (degree of polymerization was 1750 ± 50) was purchased from Tianjin Kaitong Chemical Reagent Co., Ltd. Water used for the preparation of the aqueous solutions was purified with a two-stage Millipore Milli-Q water purification system. Other reagents were analytically pure and used without further purification.

4.2. Synthesis of PAA-CD and PAA-Azo. The amine-modified β-CD derivative (abbreviated as NH_2-β-CD) was synthesized according to the reported literature.[39] PAA-CD was synthesized by the reaction between the amino group of NH_2-β-CD and the carboxyl group of PAA according to the reported previous studies.[59,60] Briefly, PAA (1 g, 1 equiv) was dissolved in water and NHS (3.4 g) and EDC-HCl (5.7 g) were then added under ice bath. The mixture was further stirred powerfully for 2 h, and then NH_2-β-CD (0.78 g, 0.05 equiv) was added. After stirring under ice bath for 12 h and at room temperature for the next 2 days, the solution was dialyzed in ultrapure water for 7 days with a dialysis tube (MWCO = 12 400). After dialysis, a white solid PAA-CD was obtained by freeze-drying. Following similar dehydration reaction procedures reported in the previous literature,[39] polyacrylic acid modified with 4-aminoazobenzene (PAA-Azo) was prepared.

4.3. Preparation of the Supramolecular Hydrogels. The dissolved PAA-CD and PAA-Azo solutions (20 mg/mL) were prepared by sonication for 5 min. PVA aqueous solutions with various concentrations (12.5, 25, 37.5, and 50 mg/mL) were prepared and constantly stirred at 90 °C for 30 min. Then, the PAA-CD solutions (0.5 mL) and PAA-Azo solutions (0.5 mL) were mixed with the different concentrations of PVA solutions (1 mL) in a thermostatic bath at 80 °C for 10 min. Then, the mixture was kept at room temperature for 2 h, and the

https://dx.doi.org/10.1021/acsomega.0c00076
ACS Omega 2020, 5, 5470−5479

hydrogels were successfully prepared. The samples were named Gel-A, Gel-B, Gel-C, and Gel-D, and other details are shown in Table 1.

4.4. Swelling Behavior Experiments. To investigate the swelling behavior of the hydrogel at different pH values, the dried Gel-D was immersed into aqueous solutions (500 mL) of different pH values at room temperature until the hydrogel reached equilibrium swelling. During this experiment, water was periodically replaced several times. The swollen gel was weighed at each predetermined time. The average of three measurements was taken as the final result. The swelling ratio (SR) was calculated as follows

$$\mathrm{SR(g/g)} = \frac{w_s - w_d}{w_d}$$

where w_s and w_d represent the weight of the swollen hydrogel and the weight of the dried hydrogel, respectively.

4.5. Adsorption Test for Dye Removal. Adsorption experiments were performed by the adsorption of two organic molecules, methylene blue (MB) and rhodamine B (RhB). The hydrogel samples (20 mg) were added to each dye solution (MB, 100 mL, 5 mg/L; RhB, 50 mL, 5 mg/L). These dye solutions were stirred slowly at a constant rate at room temperature in the dark. The supernatants were taken at different time intervals for further testing using a UV−visible spectrometer. The UV−vis absorption spectra were recorded for the adsorption stage at wavelengths of 670 nm (MB) and 554 nm (RhB) to determine the concentration of dyes in the solutions. To determine the adsorption effect of dye solutions at different pH values (3−11), the initial pH values of dye solution were adjusted by using 1 M HCl and NaOH solutions.

4.6. Characterization. The xerogels used in the present study were acquired using a lyophilizer at −50 °C with an FD-1C-50 lyophilizer instrument from Beijing Boyikang Experimental Instrument Co., Ltd. (Beijing, China) to completely remove water over 2−3 days. The microstructure of the xerogels was observed by a field-emission scanning electron microscope (SEM) (S-4800II, Hitachi, Japan) with 0.5−30 kV accelerating voltage as well as transmission electron microscopy with 20 kV accelerating voltage (TEM, HT7700, Hitachi High-Technologies Corporation, Japan). X-ray diffraction (XRD) patterns were obtained on an X-ray diffractometer (SMART LAB, Rigaku; Rigaku D/MAX-2500/PC) with Cu Kα X-ray radiation. The infrared spectra were characterized by Fourier infrared spectroscopy (Nicolet Corporation) by the KBr sheet method. UV−vis absorption spectra of the samples were recorded on a 752-type UV−vis spectrometer (Sunny Hengping Scientific Instrument Co., Ltd., Shanghai, China). The specific surface area and pore size distribution were determined using Brunauer−Emmett−Teller (BET) measurements (ASAP 2460).

AUTHOR INFORMATION

Corresponding Authors

Jingxin Zhou − *Hebei Key Laboratory of Applied Chemistry, School of Environmental and Chemical Engineering, Yanshan University, Qinhuangdao 066004, P. R. China*; Email: zhoujingxin@ysu.edu.cn

Tifeng Jiao − *State Key Laboratory of Metastable Materials Science and Technology and Hebei Key Laboratory of Applied Chemistry, School of Environmental and Chemical Engineering, Yanshan University, Qinhuangdao 066004, P. R. China*; orcid.org/0000-0003-1238-0277; Email: tfjiao@ysu.edu.cn

Authors

Nan Hou − *State Key Laboratory of Metastable Materials Science and Technology and Hebei Key Laboratory of Applied Chemistry, School of Environmental and Chemical Engineering, Yanshan University, Qinhuangdao 066004, P. R. China*

Ran Wang − *Hebei Key Laboratory of Applied Chemistry, School of Environmental and Chemical Engineering, Yanshan University, Qinhuangdao 066004, P. R. China*

Fan Wang − *Hebei Key Laboratory of Applied Chemistry, School of Environmental and Chemical Engineering, Yanshan University, Qinhuangdao 066004, P. R. China*

Jiahui Bai − *Hebei Key Laboratory of Applied Chemistry, School of Environmental and Chemical Engineering, Yanshan University, Qinhuangdao 066004, P. R. China*

Lexin Zhang − *Hebei Key Laboratory of Applied Chemistry, School of Environmental and Chemical Engineering, Yanshan University, Qinhuangdao 066004, P. R. China*

Jie Hu − *Hebei Key Laboratory of Applied Chemistry, School of Environmental and Chemical Engineering, Yanshan University, Qinhuangdao 066004, P. R. China*

Shufeng Liu − *Key Laboratory of Optic-electric Sensing and Analytical Chemistry for Life Science, Ministry of Education, College of Chemistry and Molecular Engineering, Qingdao University of Science and Technology, Qingdao 266042, P. R. China*; orcid.org/0000-0003-4063-4537

Complete contact information is available at: https://pubs.acs.org/10.1021/acsomega.0c00076

Notes

The authors declare no competing financial interest.

ACKNOWLEDGMENTS

This work was financially supported by the National Natural Science Foundation of China (No. 21872119), the Talent Engineering Training Funding Project of Hebei Province (No. A201905004), the Research Program of the College Science and Technology of Hebei Province (No. ZD2018091), and the Hebei Province Graduate Innovation Funding Project (No. CXZZSS2020047).

REFERENCES

(1) Hoare, T. R.; Kohane, D. S. Hydrogels in drug delivery: Progress and challenges. *Polymer* **2008**, *49*, 1993−2007.

(2) Zhang, J.; Ma, P. X. Cyclodextrin-based supramolecular systems for drug delivery: recent progress and future perspective. *Adv. Drug Delivery Rev.* **2013**, *65*, 1215−1233.

(3) Feng, S.; Li, Q.; Wang, S.; Wang, B.; Hou, Y.; Zhang, T. Tunable Dual Temperature-Pressure Sensing and Parameter Self-Separating Based on Ionic Hydrogel via Multisynergistic Network Design. *ACS Appl. Mater. Interfaces* **2019**, *11*, 21049−21057.

(4) Xing, R.; Liu, K.; Jiao, T.; Zhang, N.; Ma, K.; Zhang, R.; Zou, Q.; Ma, G.; Yan, X. An Injectable Self-Assembling Collagen-Gold Hybrid Hydrogel for Combinatorial Antitumor Photothermal/Photodynamic Therapy. *Adv. Mater.* **2016**, *28*, 3669−3676.

(5) Hou, N.; Wang, R.; Geng, R.; Wang, F.; Jiao, T.; Zhang, L.; Zhou, J.; Bai, Z.; Peng, Q. Facile preparation of self-assembled hydrogels constructed from poly-cyclodextrin and poly-adamantane as highly selective adsorbents for wastewater treatment. *Soft Matter* **2019**, *15*, 6097−6106.

(6) Soleimani, K.; Tehrani, A. D.; Adeli, M. Preparation of new GO-based slide ring hydrogel through a convenient one-pot approach as methylene blue absorbent. *Carbohydr. Polym.* **2018**, *187*, 94−101.

(7) Nakahata, M.; Takashima, Y.; Yamaguchi, H.; Harada, A. Redox-responsive self-healing materials formed from host-guest polymers. *Nat. Commun.* **2011**, *2*, No. 511.
(8) Song, M. M.; Wang, Y. M.; Wang, B.; Liang, X. Y.; Chang, Z. Y.; Li, B. J.; Zhang, S. Super Tough, Ultrastretchable Hydrogel with Multistimuli Responsiveness. *ACS Appl. Mater. Interfaces* **2018**, *10*, 15021−15029.
(9) Le, X.; Lu, W.; Zheng, J.; Tong, D.; Zhao, N.; Ma, C.; Xiao, H.; Zhang, J.; Huang, Y.; Chen, T. Stretchable supramolecular hydrogels with triple shape memory effect. *Chem. Sci.* **2016**, *7*, 6715−6720.
(10) Lin, P.; Ma, S.; Wang, X.; Zhou, F. Molecularly engineered dual-crosslinked hydrogel with ultrahigh mechanical strength, toughness, and good self-recovery. *Adv. Mater.* **2015**, *27*, 2054−2059.
(11) Kakuta, T.; Takashima, Y.; Harada, A. Highly Elastic supramolecular Hydrogels Using Host−Guest Inclusion Complexes with cyclodextrins. *Macromolecules* **2013**, *46*, 4575−4579.
(12) Liu, T.; Jiao, C.; Peng, X.; Chen, Y.-N.; Chen, Y.; He, C.; Liu, R.; Wang, H. Super-strong and tough poly(vinyl alcohol)/poly(acrylic acid) hydrogels reinforced by hydrogen bonding. *J. Mater. Chem. B* **2018**, *6*, 8105−8114.
(13) Burattini, S.; Greenland, B.; Merino, D.; Weng, W.; Seppala, J.; Colquhoun, H. M.; Hayes, W.; Mackay, M.; Hamley, I.; Rowan, S. A healable supramolecular polymer blend based on aromati π-π stacking and hydrogen-bonding interactions. *J. Am. Chem. Soc.* **2010**, *132*, 12051−12058.
(14) Peng, F.; Li, G.; Liu, X.; Wu, S.; Tong, Z. Redox-Responsive Gel-Sol/Sol-Gel Transition in Poly(acrylic acid) Aqueous Solution Containing Fe(III) Ions Switched by Light. *J. Am. Chem. Soc.* **2008**, *130*, 16166−16167.
(15) Shen, J.; Pang, J.; Kalwarczyk, T.; Hołyst, R.; Xin, X.; Xu, G.; Luan, X.; Yang, Y. Manipulation of multiple-responsive fluorescent supramolecular materials based on the inclusion complexation of cyclodextrins with Tyloxapol. *J. Mater. Chem. C* **2015**, *3*, 8104−8113.
(16) Shen, J.; Xin, X.; Zhang, Y.; Song, L.; Wang, L.; Tang, W.; Ren, Y. Manipulation the behavior of supramolecular hydrogels of α-cyclodextrin/star-like block copolymer/carbon-based Nanomaterials. *Carbohydr. Polym.* **2015**, *117*, 592−599.
(17) Shen, J.; Xin, X.; Liu, T.; Tong, L.; Xu, G.; Yuan, S. Manipulation the properties of supramolecular hydrogels of α-cyclodextrin/Tyloxapol/carbon-based Nanomaterials. *J. Colloid Interface Sci.* **2016**, *468*, 78−85.
(18) Shen, J.; Song, L.; Xin, X.; Wu, D.; Wang, S.; Chen, R.; Xu, G. Self-assembled supramolecular hydrogel induced by β-cyclodextrin and ionic liquid-type imidazolium gemini surfactant. *Colloids Surf., A* **2016**, *509*, 512−520.
(19) Harada, A.; Takashima, Y.; Nakahata, M. supramolecular polymeric materials via cyclodextrin-guest interactions. *Acc. Chem. Res.* **2014**, *47*, 2128−2140.
(20) He, L.; Huang, J.; Chen, Y.; Xu, X.; Liu, L. Inclusion Interaction of Highly Densely PEO Grafted Polymer Brush and R-cyclodextrin. *Macromolecules* **2005**, *38*, 3845−3851.
(21) Cheng, W.; Zhao, D.; Qiu, Y.; Hu, H.; Wang, H.; Wang, Q.; Liao, Y.; Peng, H.; Xie, X. Robust multi-responsive supramolecular hydrogel based on a mono-component host-guest gelator. *Soft Matter* **2018**, *14*, 5213−5221.
(22) Wang, X.; Wang, J.; Yang, Y.; Yang, F.; Wu, D. Fabrication of multi-stimuli responsive supramolecular hydrogels based on host−guest inclusion complexation of a tadpole-shaped cyclodextrin derivative with the azobenzene dimer. *Polym. Chem.* **2017**, *8*, 3901−3909.
(23) Zhu, J.; Wang, R.; Geng, R.; Zhang, X.; Wang, F.; Jiao, T.; Yang, J.; Bai, Z.; Peng, Q. A facile preparation method for new two-component supramolecular hydrogels and their performances in adsorption, catalysis, and stimuli-response. *RSC Adv.* **2019**, *9*, 22551−22558.
(24) Pandey, S.; Do, J.; Kim, J.; Kang, M. Fast and highly efficient catalytic degradation of dyes using κ-carrageenan stabilized silver nanoparticles nanocatalyst. *Carbohydr. Polym.* **2020**, *230*, No. 115597.
(25) Thakur, S.; Pandey, S.; Arotiba, O. Development of a sodium alginate-based organic/inorganic superabsorbent composite hydrogel for adsorption of methylene blue. *Carbohydr. Polym.* **2016**, *153*, 34−46.
(26) Guo, R.; Jiao, T.; Li, R.; Chen, Y.; Guo, W.; Zhang, L.; Zhou, J.; Zhang, Q.; Peng, Q. Sandwiched Fe_3O_4/Carboxylate graphene Oxide Nanostructures Constructed by Layer-by-Layer Assembly for Highly Efficient and Magnetically Recyclable Dye Removal. *ACS Sustainable Chem. Eng.* **2018**, *6*, 1279−1288.
(27) Pandey, S.; Do, J.; Kim, J.; Kang, M. Fast and highly efficient removal of dye from aqueous solution using natural locust bean gum based hydrogels as adsorbent. *Int. J. Biol. Macromol.* **2020**, *143*, 60−75.
(28) Pandey, S. A comprehensive review on recent developments in bentonite-based materials used as adsorbents for wastewater treatment. *J. Mol. Liq.* **2017**, *241*, 1091−1113.
(29) Makhado, E.; Pandey, S.; Ramontja, J. Microwave-assisted green synthesis of xanthan gum grafted diethylamino ethyl methacrylate: An efficient adsorption of hexavalent chromium. *Carbohydr. Polym.* **2019**, *222*, No. 114989.
(30) Nakhjiri, M. T.; Marandi, G. B.; Kurdtabar, M. Poly(AA-co-VPA) hydrogel cross-linked with N-maleyl chitosan as dye adsorbent: Isotherms, kinetics and thermodynamic investigation. *Int. J. Biol. Macromol.* **2018**, *117*, 152−166.
(31) Hu, X. S.; Liang, R.; Sun, G. Super-adsorbent hydrogel for removal of methylene blue dye from aqueous solution. *J. Mater. Chem. A* **2018**, *6*, 17612−17624.
(32) Gao, Y.; Guo, R.; Feng, Y.; Zhang, L.; Wang, C.; Song, J.; Jiao, T.; Zhou, J.; Peng, Q. Self-Assembled Hydrogels Based on Poly-cyclodextrin and Poly-azobenzene Compounds and Applications for Highly Efficient Removal of Bisphenol A and Methylene Blue. *ACS Omega* **2018**, *3*, 11663−11672.
(33) Gong, Z.; Zhang, G.; Zeng, X.; Li, J.; Li, G.; Huang, W.; Sun, R.; Wong, C. High-Strength, Tough, Fatigue Resistant, and Self-Healing Hydrogel Based on Dual Physically Cross-Linked Network. *ACS Appl. Mater. Interfaces* **2016**, *8*, 24030−24037.
(34) Iwaso, K.; Takashima, Y.; Harada, A. Fast response dry-type artificial molecular muscles with [c2]daisy chains. *Nat. Chem.* **2016**, *8*, 625−632.
(35) Hou, N.; Wang, R.; Wang, F.; Bai, J.; Jiao, T.; Bai, Z.; Zhang, L.; Zhou, J.; Peng, Q. Self-assembled hydrogels constructed via host-guest polymers with highly efficient dye removal capability for wastewater treatment. *Colloids Surf., A* **2019**, *579*, No. 123670.
(36) Hou, C.; Ma, K.; Jiao, T.; Xing, R.; Li, K.; Zhou, J.; Zhang, L. Preparation and dye removal capacities of porous silver nanoparticle-containing composite hydrogels via poly(acrylic acid) and silver ions. *RSC Adv.* **2016**, *6*, 110799−110807.
(37) Takeshita, J.; Hasegawa, Y.; Yanai, K.; Yamamoto, A.; Ishii, A.; Hasegawa, M.; Yamanaka, M. Organic Dye Adsorption by Amphiphilic Tris-Urea supramolecular Hydrogel. *Chem. - Asian J.* **2017**, *12*, 2029−2032.
(38) Singha, N. R.; Mahapatra, M.; Karmakar, M.; Dutta, A.; Mondal, H.; Chattopadhyay, P. K. Synthesis of guar gum-g-(acrylic acid-co-acrylamide-co-3-acrylamido propanoic acid) IPN via in situ attachment of acrylamido propanoic acid for analyzing superadsorption mechanism of Pb(ii)/Cd(ii)/Cu(ii)/MB/MV. *Polym. Chem.* **2017**, *8*, 6750−6777.
(39) Yan, B.; Chen, Z.; Cai, L.; Chen, Z.; Fu, J.; Xu, Q. Fabrication of polyaniline hydrogel: Synthesis, characterization and adsorption of methylene blue. *Appl. Surf. Sci.* **2015**, *356*, 39−47.
(40) Quan, C. Y.; Chen, J. X.; Wang, H. Y.; Li, C.; Chang, C.; Zhang, X. Z.; Zhuo, R. X. Core-shell nanosized assemblies mediated by the α-β cyclodextrin dimer with a tumor-triggered targeting property. *ACS Nano* **2010**, *4*, 4211−4219.
(41) Wang, C.; Yin, J.; Han, S.; Jiao, T.; Bai, Z.; Zhou, J.; Zhang, L.; Peng, Q. Preparation of Palladium Nanoparticles Decorated Poly-ethyleneimine/Polycaprolactone Composite Fibers Constructed by electrospinning with Highly Efficient and Recyclable Catalytic Performances. *Catalysts* **2019**, *9*, No. 559.
(42) Ma, K.; Chen, W.; Jiao, T.; Jin, X.; Sang, Y.; Yang, D.; Zhou, J.; Liu, M.; Duan, P. Boosting Circularly Polarized Luminescence of Small

https://dx.doi.org/10.1021/acsomega.0c00076
ACS Omega 2020, 5, 5470−5479

Organic Molecules via Multi-dimensional Morphology Control. *Chem. Sci.* **2019**, *10*, 6821−6827.
(43) He, Y.; Wang, R.; Jiao, T.; Yan, X.; Wang, M.; Zhang, L.; Bai, Z.; Zhang, Q.; Peng, Q. Facile Preparation of Self-Assembled Layered Double Hydroxide-Based Composite Dye Films as New Chemical Gas Sensors. *ACS Sustainable Chem. Eng.* **2019**, *7*, 10888−10899.
(44) Ma, K.; Wang, R.; Rao, Y.; Zhao, W.; Liu, S.; Jiao, T. Langmuir-Blodgett films of two chiral perylene bisimide-based molecules: aggregation and supramolecular chirality. *Colloids Surf., A* **2020**, *591*, No. 124563.
(45) Feng, Y.; Yin, J.; Liu, S.; Wang, Y.; Li, B.; Jiao, T. Facile Synthesis of Ag/Pd Nanoparticles-Loaded Polyethyleneimine Composite Hydrogels with Highly Efficient Catalytic Reduction of 4-Nitrophenol. *ACS Omega* **2020**, *5*, 3725−3733.
(46) He, Y.; Wang, R.; Sun, C.; Liu, S.; Zhou, J.; Zhang, L.; Jiao, T.; Peng, Q. Facile Synthesis of Self-Assembled NiFe Layered Double Hydroxide-Based azobenzene Composite Films with Photo-Isomerization and Chemical Gas Sensor Performances. *ACS Omega* **2020**, *5*, 3689−3698.
(47) Song, J.; Yuan, C.; Jiao, T.; Xing, R.; Yang, M.; Adams, D. J.; Yan, X. Multifunctional Antimicrobial Biometallohydrogels Based on Amino Acid Coordinated Self-Assembly. *Small* **2020**, *16*, No. 1907309.
(48) Zhang, L.; Yin, J.; Wei, K.; Li, B.; Jiao, T.; Chen, Y.; Zhou, J.; Peng, Q. Fabrication of hierarchical $SrTiO_3$@MoS_2 heterostructure nanofibers as efficient and low-cost Electrocatalyst for hydrogen evolution reaction. *Nanotechnology* **2020**, *31*, No. 205604.
(49) Cai, C.; Wang, R.; Liu, S.; Yan, X.; Zhang, L.; Wang, M.; Tong, Q.; Jiao, T. Synthesis of Self-Assembled Phytic Acid-MXene nanocomposites via a Facile Hydrothermal Approach with Elevated Dye Adsorption Capacities. *Colloids Surf., A* **2020**, *589*, No. 124468.
(50) Xu, Y.; Wang, R.; Zheng, Y.; Zhang, L.; Jiao, T.; Peng, Q.; Liu, Z. Facile Preparation of Self-Assembled Ni/Co Phosphates Composite Spheres with Highly Efficient HER Electrocatalytic Performances. *Appl. Surf. Sci.* **2020**, *509*, No. 145383.
(51) Geng, R.; Yin, J.; Zhou, J.; Jiao, T.; Feng, Y.; Zhang, L.; Chen, Y.; Bai, Z.; Peng, Q. In Situ Construction of Ag/TiO_2/g-C_3N_4 Heterojunction Nanocomposite Based on Hierarchical Co-Assembly with Sustainable Hydrogen Evolution. *Nanomaterials* **2020**, *10*, No. 1.
(52) Zhan, F.; Yin, J.; Zhou, J.; Jiao, T.; Zhang, L.; Xia, M.; Bai, Z.; Peng, Q. Facile preparation and highly efficient catalytic performances of Pd-Cu bimetallic catalyst synthesized via Seed-mediated method. *Nanomaterials* **2020**, *10*, No. 6.
(53) Feng, Y.; Wang, R.; Yin, J.; Zhan, F.; Chen, K.; Jiao, T.; Zhou, J.; Zhang, L.; Peng, Q. Facile Synthesis of Cu_2O nanoparticle-loaded Carbon Nanotubes Composite Catalysts for Reduction of 4-Nitrophenol. *Curr. Nanosci.* **2020**, DOI: 10.2174/1573413715666191206161555.
(54) Li, H.; Yin, J.; Meng, Y.; Liu, S.; Jiao, T. Nickel/Cobalt-Containing polypyrrole Hydrogel-Derived Approach for Efficient ORR Electrocatalyst. *Colloids Surf., A* **2020**, *586*, No. 124221.
(55) Zhao, J.; Yin, J.; Zhong, J.; Jiao, T.; Bai, Z.; Wang, S.; Zhang, L.; Peng, Q. Facile preparation of a self-assembled artemia cyst shell−TiO_2−MoS_2 porous composite structure with highly efficient catalytic reduction of nitro compounds for wastewater treatment. *Nanotechnology* **2020**, *31*, No. 085603.
(56) Meng, Y.; Yin, J.; Jiao, T.; Bai, J.; Zhang, L.; Su, J.; Liu, S.; Bai, Z.; Cao, M.; Peng, Q. Self-assembled copper/cobalt-containing polypyrrole hydrogels for highly efficient ORR electrocatalysts. *J. Mol. Liq.* **2020**, *298*, No. 112010.
(57) Yin, J.; Zhan, F.; Jiao, T.; Deng, H.; Zou, G.; Bai, Z.; Zhang, Q.; Peng, Q. Highly efficient catalytic performances of nitro compounds via hierarchical PdNPs-loaded MXene/polymer nanocomposites synthesized through electrospinning strategy for wastewater treatment. *Chin. Chem. Lett.* **2020**, DOI: 10.1016/j.cclet.2019.08.047.
(58) Ma, K.; Wang, R.; Jiao, T.; Zhou, J.; Zhang, L.; Li, J.; Bai, Z.; Peng, Q. Preparation and aggregate state regulation of co-assembly graphene oxide-porphyrin composite Langmuir films via surface-modified graphene oxide sheets. *Colloids Surf., A* **2020**, *584*, No. 124023.
(59) Gao, Y.; Jiao, T.; Ma, K.; Xing, R.; Zhang, L.; Zhou, J.; Peng, Q. Variable self-assembly and in situ host−guest reaction of beta-cyclodextrin-modified graphene oxide composite Langmuir films with azobenzene compounds. *RSC Adv.* **2017**, *7*, 41043−41051.
(60) Xuan, H.; Ren, J.; Wang, X.; Zhang, J.; Ge, L. Flame-retardant, non-irritating and self-healing multilayer films with double-network structure. *Compos. Sci. Technol.* **2017**, *145*, 15−23.

https://dx.doi.org/10.1021/acsomega.0c00076
ACS Omega 2020, 5, 5470−5479